Determination of Effective Critical Breakdown Field in 4H-SiC Superjunction Devices

Mohamed Torky[1,a*] and T. Paul Chow[1,b]

[1]Rensselaer Polytechnic Institute, Troy, NY 12180, U.S.A.

[a]torkym@rpi.edu, [b]chowt@rpi.edu

Abstract. We determine the effective critical breakdown field for 4H-SiC superjunction (SJ) devices and compare it to their conventional counterparts. Also, we investigate its dependence on SJ device structural parameters, such as drift layer thickness (t) and pillar width (W). In 4H-SiC SJ devices, the effective critical breakdown field was found to be around 30% lower than that of conventional devices owing to their longer ionization paths. In particular, the effective critical electric field varies as $\xi_{cr} \propto t^{-1/10}$ and $\xi_{cr} \propto t^{-1/6}$ for 4H-SiC SJ and conventional devices respectively but independent of pillar width and doping concentration for high aspect ratio devices (t/W > 10).

Introduction

High voltage, vertical superjunction (SJ) power devices, which exhibit a quasi-rectangular field profile, instead of a triangular field profile, at breakdown, offer a better trade-off between breakdown voltage (BV) and specific on-resistance ($R_{on,sp}$) (ideally, $R_{on,sp} \propto BV$, instead of $R_{on,sp} \propto BV^{2.5}$) than conventional power devices [1]-[2]. In addition, wide bandgap semiconductors, like 4H-SiC, exhibit better pertinent material properties, such as 10× higher critical field and 3× higher thermal conductivity, than silicon. Recently, we have determined the performance limit of 4H-SiC SJ devices [3]. However, the dependence of effective critical field on the doping and the drift layer thickness in any semiconductor SJ devices is still unknown. In this paper, the effective critical field for 4H-SiC SJ devices will be determined using a device simulator (Sentaurus), so as to facilitate their BV design.

Device Design

A half unit cell of the DMOS SJ vertical power MOSFET structure is schematically shown in Fig. 1. We simplify the drift region with the idealized PIN diode structure in Fig. 2 and simulate its effective critical field with the drift layer thickness (t) ranging from 1μm to 50μm and pillar widths (W) of 0.3, 0.6, 1.2, and 2.4μm at the optimized pillar dosage (10^{13}cm^{-2}). The impact ionization coefficients in Table 1, used in the simulations, were developed by [4] and the model, the Chynoweth's model, which governs their dependence on the electric field, is shown in Eqs. (1,2).

$$\alpha_n = A_n \exp\left(-\frac{B_n}{\mathcal{E}}\right) \tag{1}$$

$$\alpha_p = A_p \exp\left(-\frac{B_p}{\mathcal{E}}\right) \tag{2}$$

Table 1. Impact ionization coefficents used in the Sentaurus TCAD [3].

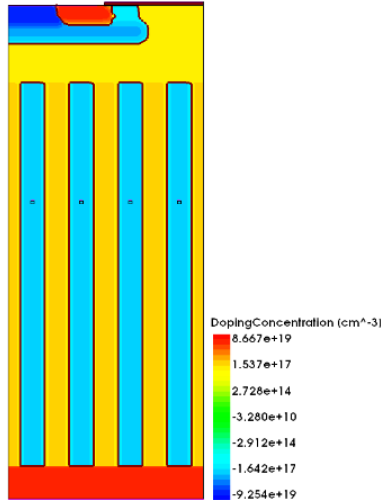| -	A_n (cm^{-1})	A_p (cm^{-1})	B_n (V/cm)	B_p (V/cm)
Values	8.19×10^9	4.48×10^6	3.94×10^7	1.01×10^6

Fig. 1. Schematic cross-section of the half unit cell of a vertical SJ DMOS FET.
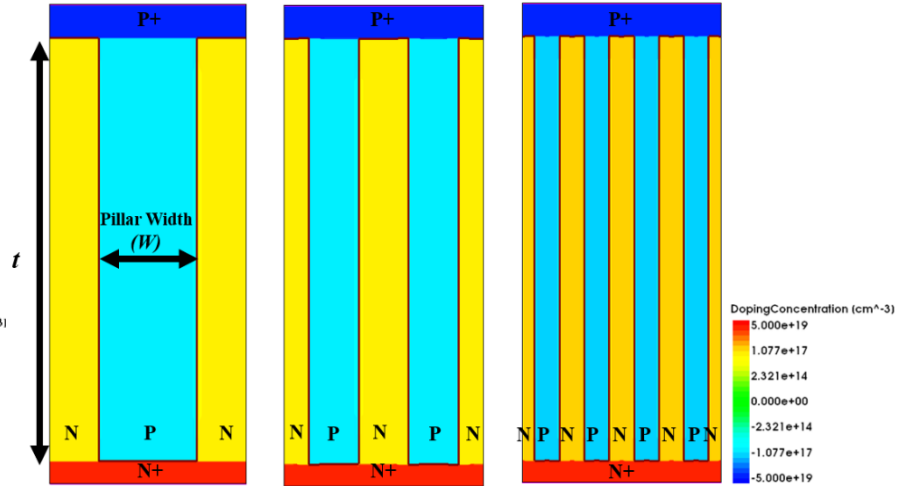
Fig. 2. Ideal PIN SJ Structures with different pillar widths.

For each power device, the electric field is simulated and extracted using Sentaurus TCAD with fine meshing along the PN junctions to account for the depletion regions. In Fig. 3, the effective critical field of the SJ devices (having a quasi-rectangular field profile) is designated as the flat region in the electric field profile, while it is the maximum value in the conventional devices (with a triangular field profile). Both the vertical and the lateral field components for the 4H-SiC SJ devices are plotted along the middle of the n-pillar in Fig. 4. The breakdown condition is reached when the total generated current density, from two-carrier simulations of the continuity equation, increases to 10^{-8} A/cm. The impact ionization rate is given by

$$G_{II} = \frac{1}{q}\left(\alpha_n . J_n + \alpha_p . J_p\right)$$
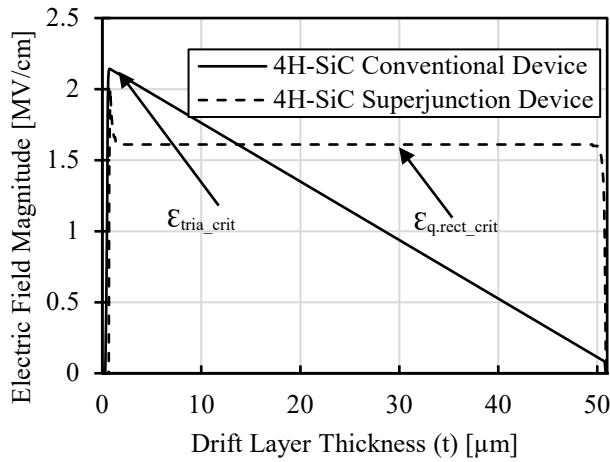
(3)

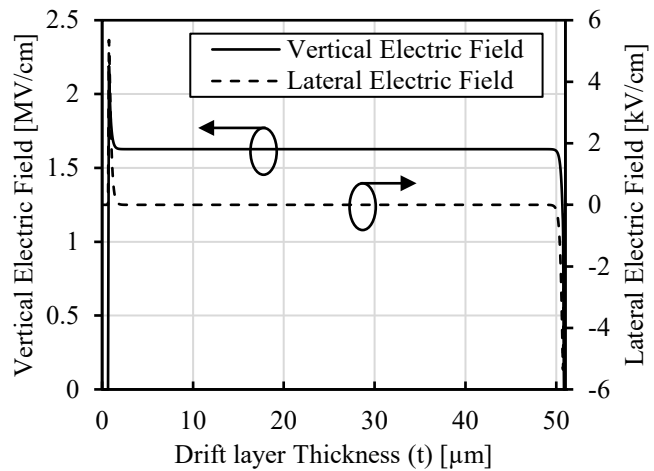Fig. 3. Electric field distribution in both conventional and SJ devices (along the middle of the n-pillar).

Fig. 4. Vertical and lateral electric field components along the middle of the n-pillar for 4H-SiC SJ devices. W=0.6µm.

In Fig. 5, the impact ionization rate is shown for both the conventional and SJ devices. It decreases rapidly for conventional devices because of the strong dependence between the impact ionization coefficients and the electric field. For the superjunction devices, the impact ionization rate is almost constant along the whole drift layer thickness because of the uniform vertical electric field along the SJ pillars. Moreover, there is a dip in the SJ impact ionization rate near the upper junction, the physical origin of this dip is the sweeping out of carriers laterally due to a finite lateral field as shown in Fig. 4. Also, since the impact ionization rate is a strong function of the electric field, in conventional devices, whose electric field profile is triangular, with the electric field decreasing linearly with the drift layer thickness, the ionization rate drops significantly (exponentially), making the ionization path to be 10% of the total drift region as shown in Fig 5. For SJ devices, the electric field is uniform along the drift layer, hence the impact ionization rate is also uniform causing a longer ionization path.
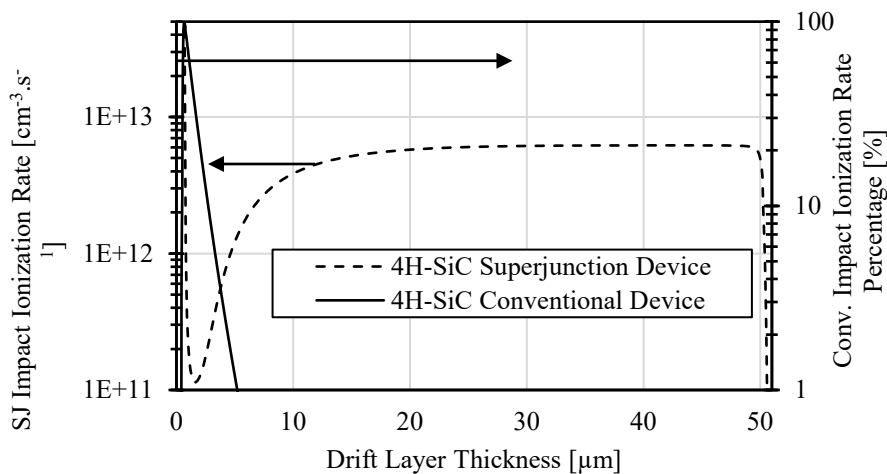

Fig. 5. Impact ionization rate along the middle of the n-pillar in both conventional and SJ devices.

Results and Discussion

The effective critical electric field has been simulated and plotted versus the drift layer thickness for conventional devices, superjunction devices, and intrinsic PIN devices as shown in Fig. 6. An ideal 1D PIN diode, whose drift region is totally intrinsic, is used here to determine the achievable electric field limit (maximum value), which the PiN SJ devices may ultimately achieve (3.9 and 2.5MV/cm for conventional and superjunction devices respectively). In Fig. 6, the effective critical field has a dependence on the drift layer thickness as $\xi_{cr} \propto t^{-1/10}$ and $\xi_{cr} \propto t^{-1/6}$ [5] for 4H-SiC conventional and superjunction devices respectively.
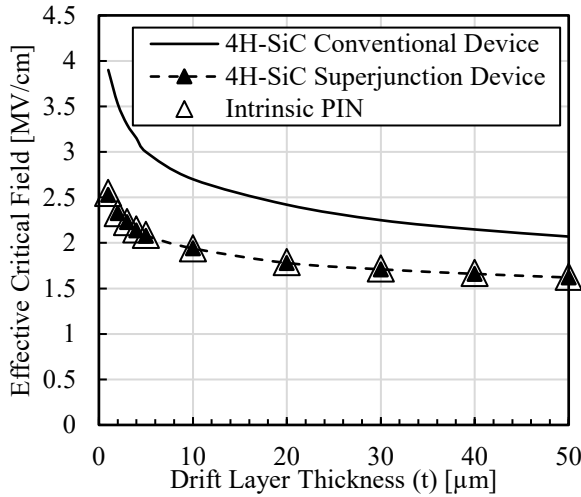
Fig. 6. A comparison between conventional and superjunction devices vs drift layer thickness (t) for 4H-SiC with intrinsic PiN results. (W=0.6μm).
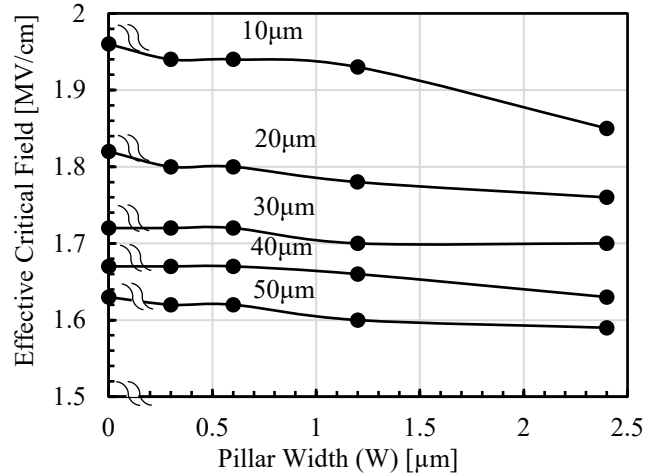
Fig. 7. Effective critical field maximum limit for 4H-SiC for different drift layer thicknesses. PiN simulation results are shown for pillar width of 0μm.

The effective critical field dependence on the pillar width with the same dosage of 10^{13} cm^{-2} is shown in Fig. 7. For SJ devices with higher aspect ratios (where t/W > 10 as shown in Fig. 2), the effective critical field is almost constant. These results show that the effective critical field has no dependence on the pillar width or pillar doping because, at avalanche breakdown, the pillars behave as an intrinsic semiconductor and the SJ diode approaches a PIN structure. The alternate P and N pillars in the superjunction (SJ) devices dictate the device to have a lateral electric field component because of which the electric field from the ionized acceptors and donors are initially terminated laterally. After the pillars are all depleted and the ions are all laterally terminated, the vertical field will be uniformly distributed along the drift layer as shown in Fig. 4.

Summary

We have determined that the effective critical electric field value of 4H-SiC SJ devices is 30% lower than that of conventional, triangular-field devices. Furthermore, the effective critical field dependence on the drift layer thickness is governed by $\xi_{cr} \propto t^{-1/10}$ and $\xi_{cr} \propto t^{-1/6}$ for 4H-SiC superjunction and conventional devices respectively, but there is no dependence on the doping or the pillar width for high aspect ratio (t/W > 10) devices.

References

[1] F. Udrea, G. Deboy, T. Fujihira, Superjunction Power Devices, History, Development, and Future Prospects, IEEE Trans. Electron Devices. 64 (2017) 713–727.

[2] B. J. Baliga, Fundamentals of Power Semiconductor Devices (Springer, New York, 2008), 358.

[3] X. Zhou, Z. B. Guo, T. P. Chow, Performance Limits of Vertical 4H-SiC and 2H-GaN Superjunction Devices, Mat. Sci. Forum. 963 (2019) 693–696.

[4] H. Niwa, J. Suda, T. Kimoto, Temperature Dependence of Impact Ionization Coefficients in 4H-SiC, Mat. Sci. Forum. 778–780 (2014) 461–466.

[5] Z. Stum, Y. Tang, H. Naik, T.P. Chow, "Improved Analytical Expressions for Avalanche Breakdown in 4H-SiC," Mat. Sci. Forum. 778-780 (2014) 467-470.